

Functionalized Graphene Nanoparticles Induce Human Mesenchymal Stem Cells to Express Distinct Extracellular Matrix Proteins Mediating Osteogenesis

This article was published in the following Dove Press journal:
International Journal of Nanomedicine

Steven D Newby^{1,2}

Tom Masi³

Christopher D Griffin⁴

William J King⁴

Anna Chipman¹

Stacy Stephenson³

David E Anderson¹

Alexandru S Biris⁴

Shawn E Bourdo⁴

Madhu Dhar¹

¹College of Veterinary Medicine, University of Tennessee, Knoxville, TN 37996, USA; ²Comparative and Experimental Medicine, University of Tennessee, Knoxville, TN 37996, USA; ³University of Tennessee Graduate School of Medicine, Knoxville, TN 37996, USA; ⁴Center for Integrative Nanotechnology Sciences, University of Arkansas at Little Rock, Little Rock, AR 72204, USA

Purpose: The extracellular matrix (ECM) labyrinthine network secreted by mesenchymal stem cells (MSCs) provides a microenvironment that enhances cell adherence, proliferation, viability, and differentiation. The potential of graphene-based nanomaterials to mimic a tissue-specific ECM has been recognized in designing bone tissue engineering scaffolds. In this study, we investigated the expression of specific ECM proteins when human fat-derived adult MSCs adhered and underwent osteogenic differentiation in the presence of functionalized graphene nanoparticles.

Methods: Graphene nanoparticles with 6–10% oxygen content were prepared and characterized by XPS, FTIR, AFM and Raman spectroscopy. Calcein-am and crystal violet staining were performed to evaluate viability and proliferation of human fat-derived MSCs on graphene nanoparticles. Alizarin red staining and quantitation were used to determine the effect of graphene nanoparticles on osteogenic differentiation. Finally, immunofluorescence assays were used to investigate the expression of ECM proteins during cell adhesion and osteogenic differentiation.

Results: Our data show that in the presence of graphene, MSCs express specific integrin heterodimers and exhibit a distinct pattern of the corresponding bone-specific ECM proteins, primarily fibronectin, collagen I and vitronectin. Furthermore, MSCs undergo osteogenic differentiation spontaneously without any chemical induction, suggesting that the physicochemical properties of graphene nanoparticles might trigger the expression of bone-specific ECM.

Conclusion: Understanding the cell–graphene interactions resulting in an osteogenic niche for MSCs will significantly improve the application of graphene nanoparticles in bone repair and regeneration.

Keywords: graphene nanoparticles, functionalized graphene, human mesenchymal stem cells, extracellular matrix, fibronectin, collagen I, osteogenic niche

Correspondence: Madhu Dhar
College of Veterinary Medicine,
University of Tennessee, Knoxville, TN
37996, USA
Tel +1865-974-5703
Fax + 1865-974-5773
Email mdhar@utk.edu

Shawn E Bourdo
Center for Integrative Nanotechnology
Sciences, University of Arkansas at Little
Rock, Little Rock, AR 72204, USA
Tel +1501-683-7222
Fax +1501-683-7601
Email sxbourdo@ualr.edu

Introduction

Bone tissue engineering scaffolds used for cell therapies function as delivery vehicles for osteoprogenitor cells to aid natural cellular and tissue behavior. These scaffolds are dynamic and their function is dependent upon the interactions between the biomaterial and the cells.¹ Cells can be endogenous and be recruited from the tissues in which the scaffold is implanted, or exogenous cells which can be delivered to the site of injury. This cell–scaffold interaction triggers pathways that can ultimately affect bone-cell formation, known as osteogenic differentiation.

Adult mesenchymal stem cells (MSCs) constitute a unique class of cells that have definite capabilities to differentiate into specialized lineages, such as an osteoblast. MSCs are spindle-shaped, fibroblast-like cells that can be isolated from bone marrow, umbilical cord blood, dental pulp, skin and adipose tissue. Isolated MSCs are adherent and can be expanded in tissue culture to generate primary cultures.^{2,3} The performance of MSCs is dependent on an assembly of biochemical, physical, and environmental factors, especially the substrate topography and the extracellular matrix (ECM). These factors allow MSCs to differentiate into osteoblasts, *in vitro* and *in vivo*, when placed in an osteogenic environment. Hence, MSCs are reliable and preferred source of osteoprogenitors.^{4,5} When MSCs are implanted *in vivo*, or seeded onto the scaffolds *in vitro*, their survival, proliferation, differentiation are dependent on the microenvironment or “niche” in which they are placed. Cell fate is dictated not only by the ECM of the environment but also by the response of the MSCs to the environment. When exogenous MSCs interact with biomimetic scaffolds, they can trigger the endogenous cells to produce ECM, or the MSCs themselves can express ECM proteins to form the matrix.^{6–9} Thus, understanding the niche signals that are triggered, for instance, evaluating the ECM that is generated when MSCs are seeded onto a scaffold and implanted in a bone defect will help the consistency and efficacy of bone tissue engineering and regenerative medicine approaches.¹⁰

During osteogenic differentiation, cells initiate the synthesis of ECM, and express osteocyte-specific markers such as alkaline phosphatase, osteopontin and osteocalcin, thus enabling the cell to progress through bone cell development. Bone ECM consists of a specific and unique organization of collagen I fibers and hydroxyapatite. Collagen I makes up more than 90% of the organic phase of bone, and the remaining 10% consists of proteins including fibronectin, laminin, vinculin and vitronectin. Fibronectin, the major non-collagenous ECM protein, is ubiquitously expressed and has a significant role in cell adhesion and differentiation. Vitronectin works with fibronectin to promote cell adhesion and proliferation at the early stages of the cell-substrate interaction processes.¹¹ Vinculin is a component of focal adhesions, and it has a major role in both the cell-to-cell and cell-to-matrix adhesion physiology. Vinculin also plays an important role in the control of the binding of actin filaments in cell adhesion to the matrix.^{8,9,11–15}

Given the importance of ECM in cellular functions, and its tissue – specificity, current strategies in bone tissue

engineering involve generating constructs that mimic the native bone ECM.¹⁶ These constructs can be generated either by adding MSCs, specific growth factors (VEGF, PDGF, etc.); coating bone-specific ECM proteins such as fibronectin and vitronectin^{17–19} onto the surface of scaffolds; or by using inherently bioactive scaffolds alone with physicochemical properties to match the native ECM. The use of specific growth factors can be expensive, and using protein coatings alone does not result in a composition, function, microstructure, and architecture that is sufficiently similar to native ECM. Therefore, the long-term goal of bone tissue engineering is to develop scaffolds that can create an “osteogenic” or “bone-specific niche” for cells by inducing the expression of bone-specific ECM proteins.

Biomaterials fabricated into nanoscale (1–100 nm) structures (nanomaterials) have been shown to mimic the native ECM and promote cell adhesion and osteogenic differentiation.^{20–22} Graphene-based nanomaterials have recently been recognized as useful components of bone tissue engineering scaffolds. Graphene derivatives are preferred over the pristine form and can be produced relatively easily by functionalization of pristine graphene, with the ultimate goal of reducing pristine graphene’s toxicity and increasing its usability in biomedical applications.^{23,24} Graphene derivatives, including nano-sheets, ribbons, and low/high/partially oxidized graphene, graphene oxide and reduced graphene oxide have varying physical and chemical properties and minimal to no toxicity.²⁵ These iterations can be used as components of biocompatible and biomimetic scaffolds for bone tissue engineering.^{26,27} Therefore, despite the concerns due to toxicity, graphene-based nanomaterials and scaffolds have been used successfully in animal and *in vitro* models of bone defects and assays.^{28–38} Even though the results of the *in vitro* assays and animal models described above are encouraging and strengthen the use of graphene derivatives in biomedicine, the biocompatibility and cytotoxicity of graphene nanoparticles is altered by parameters, such as surface functionalization, shape, size, dose, cell type, and the experimental design. As a result, more research is warranted before the nanoparticles can be used effectively in a human clinical setting.

Our group has demonstrated that a low oxygen (6–10%) functionalized form of graphene nanocomposite (LOG – low-oxygen graphene) is cytocompatible and exhibits osteoinductive effects *in vitro* and osteoconductive and osseointegrative effects *in vivo* when used with fat-derived goat MSCs.^{29,37} As previously described, the

LOG form of nanoparticles are distinct from the commercially available forms of graphene oxide and the reduced graphene oxide, or the carbon-based nanosheets.^{24,38} The aim of the current study was to evaluate the effect of low-oxygen graphene nanoparticles on cellular adhesion and osteogenic differentiation of human adipose tissue-derived MSCs (hMSCs), with a focus on the spatiotemporal expression profiles of ECM proteins during these processes. Our long-term goal is to evaluate the signaling mechanism(s) that are initiated when hMSCs are seeded on graphene nanoparticles, and the current study is the first step in that direction. We hypothesized that the structure and topographical features of functionalized graphene nanoparticles will create an “osteogenic niche” for human MSCs, which will be demonstrated by osteogenic differentiation and the expression and unique distribution pattern of ECM proteins.

Methods

Isolation, ex vivo Expansion, and Characterization of Human MSCs

Stromal vascular fraction cells were obtained from human adipose tissue from patients undergoing panniculectomies in accordance with a protocol approved by the IRB at the University of Tennessee Medical Center in Knoxville. A written, informed patient consent was obtained prior to the harvest. The hMSCs were isolated, ex vivo expanded and characterized as described previously.³⁹ All experiments were performed using cells, from passages 2 through 6 only, and were incubated in complete growth media (DMEM/F12, 1% penicillin-streptomycin/amphotericin B, 10% FBS).

MSCs obtained were confirmed by their morphology, potential to undergo tri-lineage differentiation, and expression of specific protein markers, using methods reported previously.^{4,39} In vitro experiments were carried out simultaneously on control (polystyrene or plastic) and graphitic surfaces. The control substrates were chosen as appropriate for the assays under experimentation.

In addition to the basic characterization of hMSCs, the expression of specific integrin heterodimers on their cell surface was evaluated in expanded cells. 1×10^6 of hMSCs were stained with anti-human $\alpha 2\beta 1$, $\alpha 5\beta 1$ and $\alpha V\beta 6$ (Millipore Sigma), $\alpha 9\beta 1$ and $\alpha V\beta 3$ (BioLegend), and $\alpha V\beta 5$ (Developmental Studies Hybridoma Bank, University of Iowa), and their corresponding isotype-matched controls. The manufacturer's recommended concentrations of antibodies were used. Immunophenotyping was performed as previously reported.^{39,39} Briefly cells were harvested and counted,

blocked in 1% goat serum in PBS for 20 mins at room temperature, and then stained with each primary antibody for 20 mins at room temperature in the dark. Subsequently, cells were washed with PBS, were collected by centrifugation and were incubated with either IgG1/APC or IgG2b/PE (Biolegend) secondary antibodies for 20 mins at room temperature in the dark. Finally, cells were fixed with 4% paraformaldehyde/PBS for 10 mins at room temperature in the dark. Roughly 20,000 events from each staining were analyzed using a BD FACS Calibur. The raw data were analyzed by FlowJo software.

Preparation and Characterization of Functionalized Graphene Films

Pristine graphene was modified to produce a low-oxygen functionalized form of graphene (LOG) with 6% to 10% oxygen content as reported previously.^{24,37} Briefly, graphene nanoplatelets (Product # N002-PDR, 1–1.2 nm thick, $\leq 10 \mu\text{m}$ lateral dimensions) were commercially obtained (Angstrom Materials, Dayton, OH) and subjected to an aqueous acidic environment ((conc H_2SO_4 :conc HNO_3 : DI water, volume ratio of 6:2:3) for oxidation.

For coating a surface, a 15 mg mass sample of LOG was mixed with 30 mL of 90% ethanol (200 proof, ACS reagent grade, Acros)/10%ultrapure water (18.2Mohm, 0.055uS/cm). The mixture was bath sonicated for 60 min followed by probe sonication (Sonics Vibra-cell VCX-130 equipped with 6 mm probe tip, 100% power for 60 min in pulses of 5sec ON, 5sec OFF). The dispersed material was then dropped using a micropipette onto individual 15 mm plastic coverslips or in each well of a 12 well plate, to give a coating of $0.21\text{mg}/\text{cm}^2$.

The physicochemical nature of the LOG nanoparticles was confirmed by X-ray photoelectron spectroscopy (XPS), structural analysis by Raman spectroscopy, functional group analysis by infrared (FTIR) spectroscopy, and the surface roughness after coating of substrates was evaluated using atomic force microscopy (AFM). XPS, Raman, and FTIR analyses were carried out as described previously.^{24,38} Briefly, XPS was performed on powder samples placed on double-sided tape on a glass substrate, and their elemental composition was studied using a Thermo K-alpha (Waltham, MA) XPS. IR was performed on pressed pellets made from the LOG powder sample and KBr was assessed using a Thermo Scientific FTIR Nicolet Model 6700 Spectrometer (Waltham, MA). Raman measurements were performed on samples of graphene powders placed on a silicon substrate using a 514 nm laser with Horiba Jobin Yvon LabRam 800 Micro-Raman (Edison, NJ).

For AFM, the scans were obtained using tapping mode (3.90 V) at 0.5 Hz and 256 lines, with integral gains between 0.5 and 2.5 and amplitude set point averaging around 19 nm. Three different 50 μm x 50 μm randomly selected regions (edge, middle, and the center) were selected. The scans were then analyzed for surface roughness using NanoScope Analysis 1.5 (Bruker) software. Each surface scan was analyzed with the selection command across at least two dimensions to determine average roughness (Ra) and root-mean-square (Rq).

In vitro Cell Viability and Proliferation on LOG Nanoparticles

Cell viability and proliferation of hMSCs on LOG was evaluated using two independent assays over an 8-day study period. Calcein-am fluorescence imaging, and crystal violet staining and quantitation were used, as described previously.^{40,41}

Cell viability on LOG was assessed using calcein-am staining as per the manufacturer's recommendations. Briefly, $25 \times 10^3/\text{cm}^2$ hMSCs were seeded on LOG and control substrates and were incubated with a 2 $\mu\text{g}/\text{mL}$ calcein-am/dimethyl sulfoxide mix in HBSS at 37° for 5 mins at 2, 4, 6 and 8 days post seeding. Green fluorescent staining was visualized and imaged using All-in-one Microscope BZ-X700 (Keyence).

Crystal violet staining and quantitation were used to determine changes in cell mass reflecting cell proliferation.⁴⁰ For staining, at 2, 4, 6 and 8 days post-seeding, cells were fixed for 10 min with 4% paraformaldehyde/PBS. The fixed cells were stained with a 0.1% crystal violet solution in deionized water for 30 min at room temperature then washed three times with deionized water. Crystal violet-stained cells were visualized and imaged using All-in-one Microscope BZ-X700 (Keyence). For quantitation, the stain was dissolved in 10% acetic acid and quantified by measuring the absorbance at 595 nm (Synergy HT). Data were plotted and statistics performed in Prism (Graphpad).

Osteogenic Differentiation and Mineralization

For osteogenic differentiation, hMSCs at a seeding density of 25×10^3 cells/ cm^2 were induced to undergo differentiation by being exposed to complete growth media supplemented with 100nM dexamethasone, 10nM β -glycerophosphate and 155 μM ascorbic acid. At 21 days, cells were fixed in 4% paraformaldehyde/PBS for 10 mins at room temperature and stained with alizarin red to detect calcium in the osteoblasts.

The accumulation of calcium in hMSCs was quantitated by the elution of alizarin red dye with 10% cetylpyridinium chloride and the color was read at 570 nm.⁴² Background readings due to the substrates alone without any cells were subtracted from the sample readings to eliminate nonspecific values. Data were plotted and statistics performed in Prism (Graphpad).

Cytoskeletal Organization and ECM Proteins

Cytoskeletal organization and MSC morphology were assessed by evaluating the expression patterns of F-actin and vimentin using previously reported methods.³⁹ The expression of ECM proteins during cell attachment (ie within 24 hrs of seeding) and osteogenic differentiation (21 days after seeding) was assessed qualitatively by immunofluorescence detection assays. A panel of ECM proteins was used. Two distinct fibronectin antibodies, 181 and 182, vitronectin, collagen I and II, laminin and vinculin were used. Briefly, hMSCs at specified time points were fixed with 4% paraformaldehyde at room temperature for 10 mins, permeabilized with 0.1% Triton X-100 in HBSS at room temperature for 10 mins, and subsequently blocked with the Universal Blocking Reagent (BioGenex) for 30 mins at room temperature. Cells were incubated with 1–2 μg of all primary antibodies and samples were incubated at 4°C for 24 hrs. Alexa Fluor 594 phalloidin (A12381; Invitrogen), Vimentin (#550513; BD Pharmingen), Collagen I (#ab3470; Abcam), Collagen II (#ab34712; Abcam), Fibronectin 181 (MAB19172; R&D Systems), Fibronectin 182 (#MAB19182; R&D Systems), Vinculin (#ab129002; Abcam), Vitronectin (#ab113700; Abcam), and Laminin (#MAB2144; R&D Systems). The cells were washed and incubated with appropriate Alexa Fluor – labelled secondary anti-mouse or anti-rabbit antibodies at room temperature for 30 mins in dark. Alexa Fluor 594 Phalloidin was pre-conjugated and hence, did not require any secondary antibody treatment step. The cells were washed twice and mounted on microscope slides with a drop of Prolong Gold antifade reagent with 4', 6-diamidino-2-phenylindole (DAPI; Molecular Probes by Life Technologies). The cells were analyzed under a fluorescence microscope (Leica DMI8).

Results

Pristine Graphene Was Functionalized to Produce LOG Nanoparticles

Pristine graphene was functionalized to improve dispersibility, and a form containing 6% to 10% oxygen was synthesized. This is referred to as low-oxygen graphene (LOG).

The LOG nanoparticles used in these experiments are distinct from commercially available graphene oxide and reduced graphene oxide forms, and have been extensively characterized and distinguished from the other forms, as described previously.^{24,38} The functionalized form of graphene was characterized by a variety of physicochemical techniques (Figure 1). The XPS spectrum in Figure 1A, shows distinct photoemission peaks corresponding to C1s at 284.8eV, O1s at 533eV, N1s at 405eV, S2p at 164eV, with an average elemental composition of 88.73% carbon, 10.57% oxygen, and <0.5% of nitrogen and sulfur (remaining from reagents used during the oxidation procedure), confirming that the synthesized form of graphene nanoparticles are indeed LOG. Further details from the XPS spectrum demonstrate the types of functional groups present in the samples. Both carbon (C1s) and oxygen (O1s) narrow scan spectra were collected and analyzed (Figure 1B and C). After completing a fitting analysis, the C1s narrow scan exhibited peaks at 248.78eV (aliphatic/aromatic C), 286.14eV (C-O), 287.26eV (C=O), 288.83eV (carboxyl, O-C=O), and 290.70 eV for π - π^* shakeup satellite peak. For the oxygen scan (O1s), two main underlying peaks are present at 532.06eV for O-C and 533.69eV for O=C.^{43,44} This data suggests a predominantly carbon-rich sample with hydroxyl, carbonyl, and carboxyl functional groups on the surface.

In addition to XPS, Raman and infrared spectroscopy were used to characterize the graphene material. Raman spectroscopy provides information on the lattice structure of the materials and the results are displayed in Figure 1D. The main spectral features are observed at approximately 1350 cm^{-1} , 1600 cm^{-1} , and 2700 cm^{-1} corresponding to the D-, G-, and 2D-bands, respectively.⁴⁵ By analyzing the intensity of the D- and G-bands, the defect nature of the material was determined. The nanoparticles generated in this study displayed an I_D/I_G ratio of 1.34, which is consistent with other published reports from our group on this form of graphene. The FTIR spectra shown in Figure 1E provided evidence of oxygen functional groups, such as hydroxyl groups by stretching mode at $\sim 3400\text{ cm}^{-1}$ and bending mode at $\sim 1400\text{ cm}^{-1}$. Carbon-hydrogen and C-OH stretches are seen in the $2950\text{--}2850\text{ cm}^{-1}$ region and in the $1200\text{--}1050\text{ cm}^{-1}$ region, respectively. Carbonyl stretching mode was present at $\sim 1720\text{ cm}^{-1}$, with sp^2 stretching from the extensive hexagonal carbon framework observed at 1630 cm^{-1} .⁴⁶ These vibrational modes observed in FTIR, coupled with results from Raman and XPS confirm that the synthesized form of graphene nanoparticles are indeed LOG as described previously.^{24,38,47}

LOG Nanoparticles Exhibit Rough Surface

Surface roughness was evaluated using atomic force microscopy (AFM, Figure 2). AFM images show that the LOG surface had mean roughness values of $\sim 630\text{ nm Rq}$ (or RMS, root-mean-square) and $\sim 460\text{ nm Ra}$ (average roughness), suggesting potential sites for cell attachment.

Progenitor Cells are MSCs and Express Specific Integrin Heterodimers

Fibroblast morphology and tri-lineage differentiation patterns of primary cultures were generated from the human stromal vascular fraction to confirm the MSC nature of cells as described previously.³⁹ Of relevance to this study, the integrin heterodimer profile of MSCs was compared between tissue culture polystyrene substrate and LOG surfaces. Data show that the expression pattern is conserved on both substrates (Supplementary Figure 1). Specifically, there was a >90% expression of $\alpha 2\beta 1$, $\alpha V\beta 5$, $\alpha 5\beta 1$ and $\alpha 5\beta 3$ heterodimers on both surfaces, suggesting that the adhesion of hMSCs on the LOG surface is similar to that of the polystyrene surface and could be mediated via any one or a combination of these heterodimeric integrin subunits.

LOG Surface Is Cytocompatible

Calcein-am staining and fluorescence imaging were used to confirm cell viability as well as the distribution of hMSCs on the LOG surface at specific time points (Figure 3A). Calcein-am is a fluorogenic, cell-permeant probe that indicates cellular health. Native Calcein-am is non-fluorescent, and shows a green fluorescence only when it reacts with the esterases that are present within live, healthy cells. As a result, the green fluorescent signal indicates cell viability. Additionally, data show that hMSCs were healthy, viable and subjectively grew in population over an 8-day period. Cells showed a distinct pattern of adhesion and clustering on LOG surfaces relative to the random distribution observed on tissue culture polystyrene substrate. This pattern could be due to the clustering of cells to specific areas of LOG surfaces or that the graphene coating in those areas is too dark to image cells. In any case, the cells that are imaged appear healthy and hence, the LOG surface was deemed cytocompatible.

Crystal violet staining (Figure 3B) and quantitation (Figure 3C) were used to evaluate cell proliferation. Data showed that cells adhered to LOG surface and proliferated with time and the cell numbers were comparable with tissue culture polystyrene substrate, further supporting

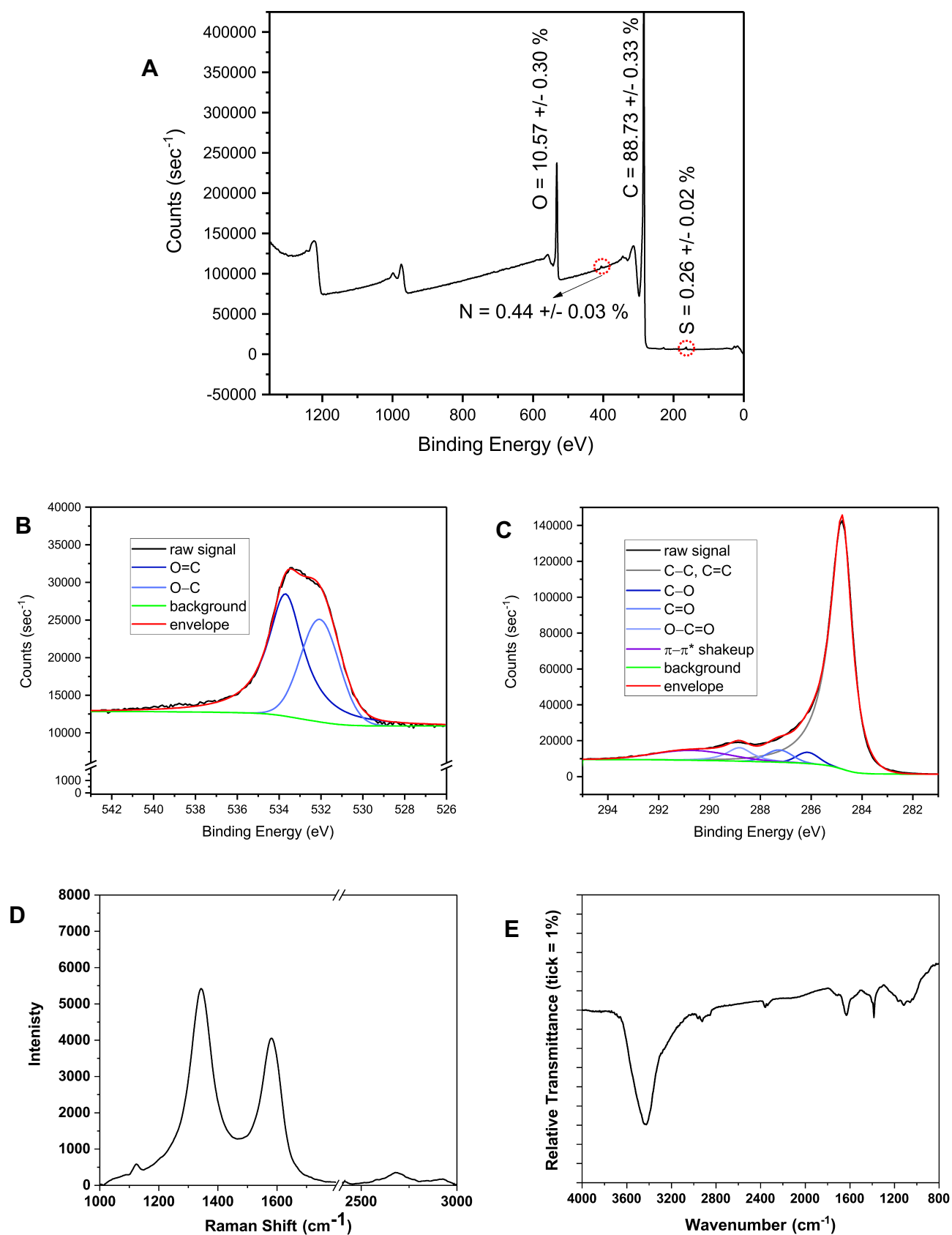


Figure 1 X-ray photoelectron spectroscopy survey scan (A), O 1s narrow scan (B), and C 1s narrow scan (C). Average atomic percent (O is oxygen as determined from O 1s peak, N is nitrogen as determined from N 1s peak, C is carbon as determined from C 1s peak, and S is sulfur as determined from S 2p peak) and standard deviation from data sets are given in the survey scan. Data collected on the low-oxygen graphene (LOG) sample by Raman spectroscopy (D) and infrared spectroscopy (E) are also displayed.

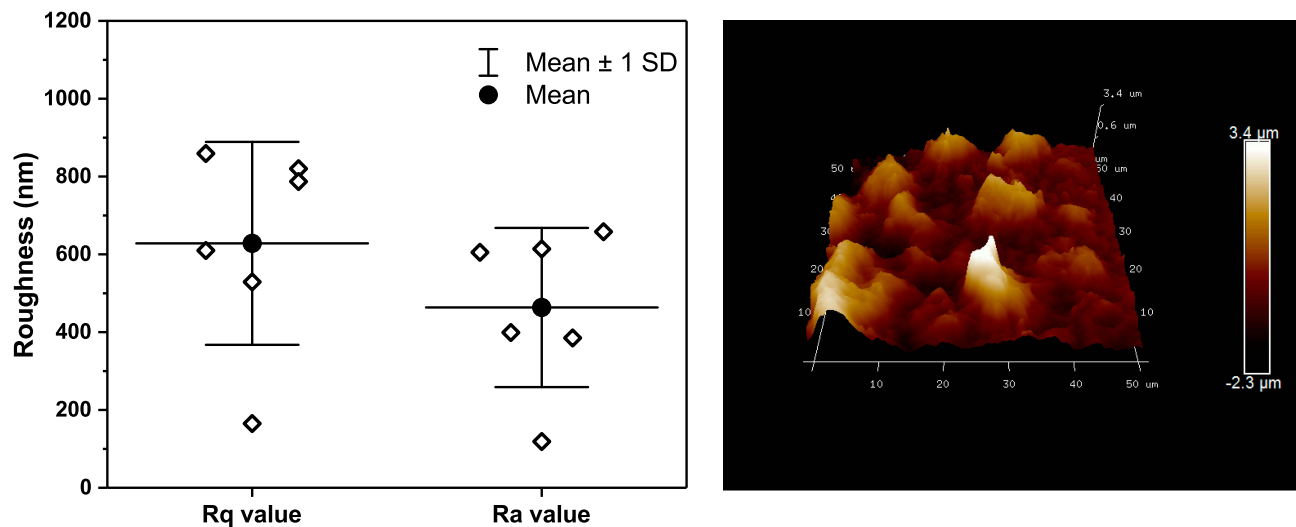


Figure 2 Atomic force microscopy. Plot of roughness values (average roughness – Ra and root-mean-square – Rq) from six atomic force microscopy (AFM) images of low-oxygen graphene (LOG) surface (Left panel) is shown. Data were obtained from 6 AFM images: data shown with diamonds, mean value with solid circle+line, and the standard deviation with whiskers. Representative AFM image from a random spot of LOG surface on glass coverslip is shown (Right panel).

the calcein-am staining and confirming the cytocompatibility of LOG surfaces.

LOG Nanoparticles Inherently Induce Osteogenic Differentiation

In view of the data from our previously published study,^{29,37} osteogenic differentiation and mineralization of hMSCs on LOG surfaces were assessed using Alizarin red staining and quantitation (Figure 4). Data show that hMSCs seeded on LOG nanoparticles demonstrated significantly greater calcium content relative to the cells on the control surface ($p=0.0018$). Interestingly, this upregulation was observed in the absence of any osteogenic inducing reagents (dexamethasone, beta-glycerophosphate or ascorbic acid), suggesting that the LOG surface induces accumulation of calcium in MSCs spontaneously, that is it induces osteogenic differentiation in vitro. Calcium content was further enhanced ($p=0.0088$) in hMSCs on LOG when osteogenic inducers were added to the media. This increase was similar and as expected to that observed in hMSCs seeded on the control surface in the presence of the osteogenic inducers ($p=0.05$), suggesting a potential synergistic effect of LOG nanoparticles and the osteogenic inducing reagents.

In order to study the osteoinductive effect of LOG nanoparticles without any interference from the osteogenic inducers, in vitro assays described below were carried out in the absence of osteogenic inducers and in growth media only. Correspondingly, to maintain the uniformity of the osteogenic status of the cells, hMSCs on the control

substrates were differentiated in the growth media supplemented with the osteogenic inducers.

Human MSCs Display Cytoskeletal Integrity on LOG Surfaces

The cytoskeletal health and integrity of the hMSCs were further confirmed on LOG surfaces by visualizing F actin filaments using a fluorescent derivative of Phalloidin (Figure 5). Fetal bovine serum in the cell media (growth and osteogenic media) is the main source of proteins that can adsorb onto a biomaterial and stimulate the production of ECM. As a result, the cytoskeletal integrity and morphology of hMSCs were evaluated in varying concentrations of FBS, ranging from 0% to 10%. Cells were fixed 24 hrs post seeding and morphological evaluation of F-actin fluorescence showed that hMSCs on LOG in media containing 2%, 5% and 10% FBS were relatively healthy and displayed robust cytoskeletal morphology. Cells in the absence of FBS (0%) appeared rounded and unhealthy. Although cells survived the 2%, 5% and 10% FBS media on LOG surface, corresponding cells on the control surface appeared unhealthy, were not viable and did not proliferate in media with <10% FBS (data not shown). In order to maintain identical cell culture conditions, hMSCs were seeded on both the control and LOG surfaces in media containing 10% FBS in all subsequent experiments. The cytoskeletal integrity of cells was first confirmed at 24 hrs during cell adhesion, and subsequently, during osteogenic differentiation at day 21 (Figure 5A).

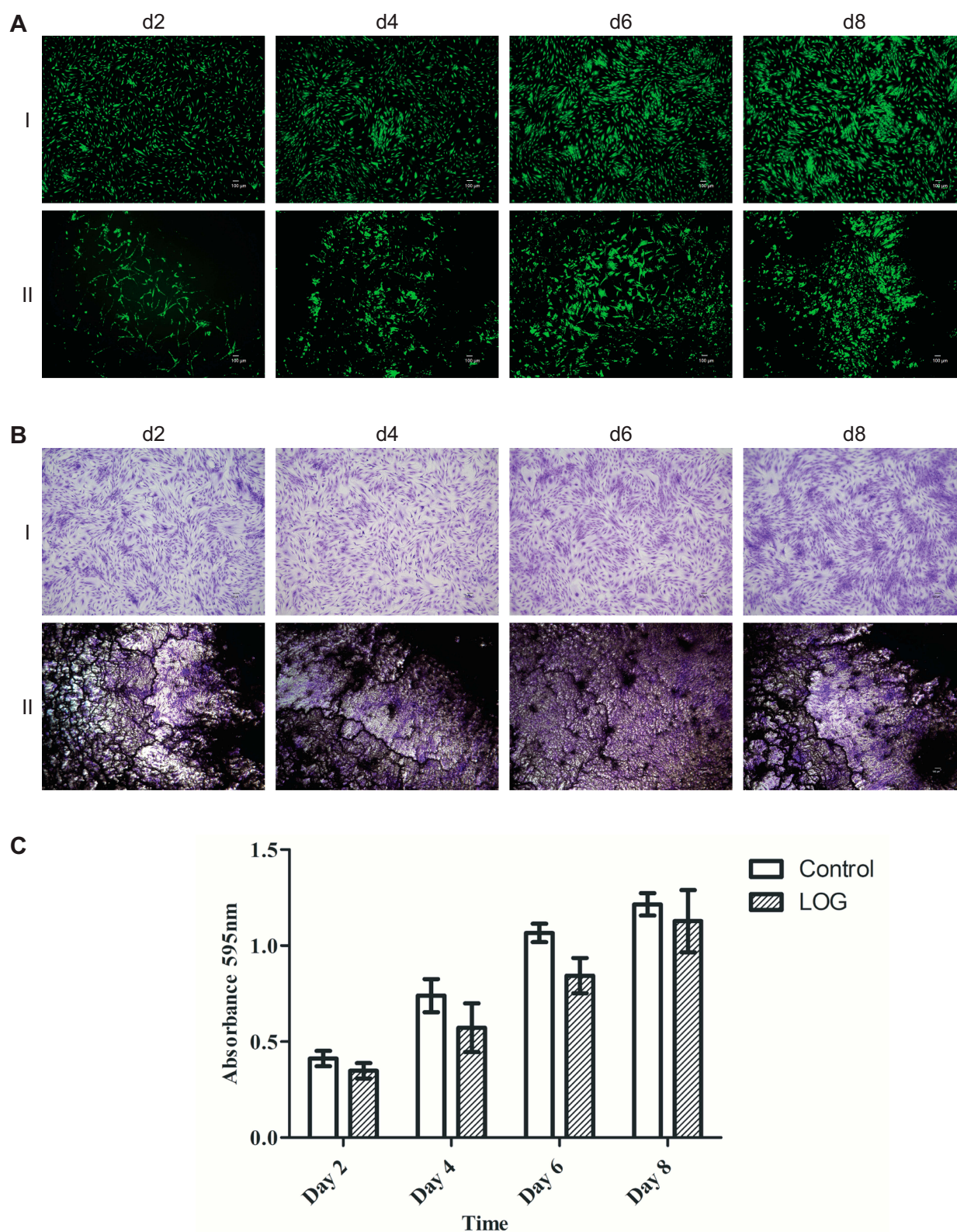


Figure 3 Cell viability staining. **(A)** Cell viability was evaluated on tissue culture polystyrene (I) and low-oxygen graphene (LOG) (II) by calcein-AM staining. Calcein-AM exhibits green fluorescence and demonstrates live cells. Fluorescent images show that human mesenchymal stem cells (hMSCs) adhered to and were viable on LOG surfaces similar to tissue culture polystyrene at all -time points. A distinct clustering of cells was, however, observed on LOG surface as early as 2 days post seeding and continued throughout the experiment on day 8. Scale bar = 100 μ m. **(B)** Indirect staining and quantitation **(C)** further confirmed cell viability and proliferation when hMSCs adhered to tissue culture polystyrene (I) and LOG (II) surfaces using crystal violet staining between days 2–8.

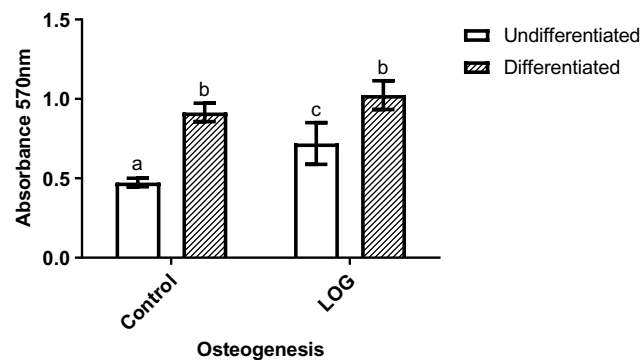


Figure 4 Osteogenic differentiation assay. Calcium content of cells that were seeded on tissue culture polystyrene (Control) and low-oxygen graphene (LOG) surfaces were visualized by Alizarin red staining and subsequently quantitated. The calcium content of cells seeded in growth media without any osteogenic inducers (undifferentiated) was compared to cells that were exposed to differentiation media (differentiated) for 21 days. Media blank, ie the tissue culture polystyrene and LOG surfaces without any cells were used as blanks and the corresponding absorbance readings were subtracted. Significantly different values ($p < 0.05$) are indicated by letters. Identical letters indicate no significance.

Simultaneous to the above experiments, we ensured that the stem cell nature of hMSCs was maintained throughout the study period by evaluating the expression of vimentin, a mesenchymal stem cell marker⁴⁸ (Figure 5B). Data confirmed that hMSCs adhered to the LOG surface and expressed vimentin confirming that hMSCs did not lose their “stem cell” characteristics during the cell culture process on LOG surfaces.

ECM Proteins are Expressed on LOG Surfaces

In order to evaluate the expression of ECM proteins that might be influenced by the serum in the media, IF assays were carried out on LOG surface in the absence of cells and only in presence of 10% FBS-containing media at 24 hrs and at day 21. The expression patterns of collagen I, collagen II, fibronectin, laminin, vinculin, and vitronectin were evaluated. IF analyses on the LOG surface did not show the expression of any ECM proteins in the absence of hMSCs in any of the samples tested, clearly demonstrating that the serum proteins do not contribute to the ECM on LOG surface and hence, do not have a role in cell adhesion or differentiation.

Next, we evaluated the expression of ECM proteins when hMSCs were seeded on the LOG surface (Figure 6). The expression patterns were evaluated at 24 hrs to assess the ECM proteins involved in cell adhesion (Figure 6A), and, at day 21, to evaluate proteins involved in osteogenic differentiation (Figure 6B). There were an expression and a discrete pattern of distribution for collagen I, fibronectin

182, vinculin and vitronectin was evident within 24-hrs post-seeding. Collagen II was weakly expressed and there was no expression of laminin, suggesting either that these proteins are not involved in adhesion and osteogenic differentiation of hMSCs on the LOG surface, or that the specific antibodies did not cross-react. Qualitatively, the distribution patterns appeared striking and discrete.

Discussion

In this study, we present in vitro data showing that in presence of functionalized graphene nanoparticles with 6–10% oxygen content, human fat-derived MSCs express and secrete a discrete and organized pattern of bone-specific ECM proteins within 24 hrs post seeding. Noteworthy is the fact that these ECM proteins were expressed in the presence of hMSCs without any contribution from the FBS present in the media. This pattern persists throughout the osteogenic differentiation process through day 21. The expression of specific ECM proteins within 24 hrs of cell seeding suggests that this phenomenon was influenced by the LOG nanoparticles, and was not a behavior of cell development or variation in culture. Our data support the earlier studies demonstrating that the expression of bone ECM – specific proteins, fibronectin, collagen I, vinculin and vitronectin affects osteogenic differentiation.^{9,12,13,18,19} For the first time, data show that these specific ECM proteins are involved in LOG nanoparticles – mediated cell adhesion and osteogenesis, which is novel and important.

Detailed evaluation of F actin staining and ECM protein expression profiles showed that hMSCs adhered, spread and covered the LOG surface within 24 hrs. Distinct areas with filipodia extensions were observed, suggesting tight cell–material interactions. Furthermore, cells arrange in multilayers, and form clusters with time, suggesting that the LOG surface offers some cell guidance, meaning attachment is not random, but organized. The clustering of hMSCs, a hallmark of osteogenic differentiation⁴⁹ further supports the commitment towards osteoblast lineage, which was confirmed via alizarin red staining and quantitation.

The cells also expressed $\alpha 2\beta 1$, $\alpha V\beta 5$, $\alpha 5\beta 1$ and $\alpha 5\beta 3$ integrin heterodimers, and, as judged by the calcium content accumulated in the cells, underwent osteogenic differentiation, suggesting that the interaction between integrin and the corresponding ECM protein partners (fibronectin and vitronectin) might mediate cell adhesion and subsequent osteogenic differentiation. These data further strengthen the observed expression of the specific ECM

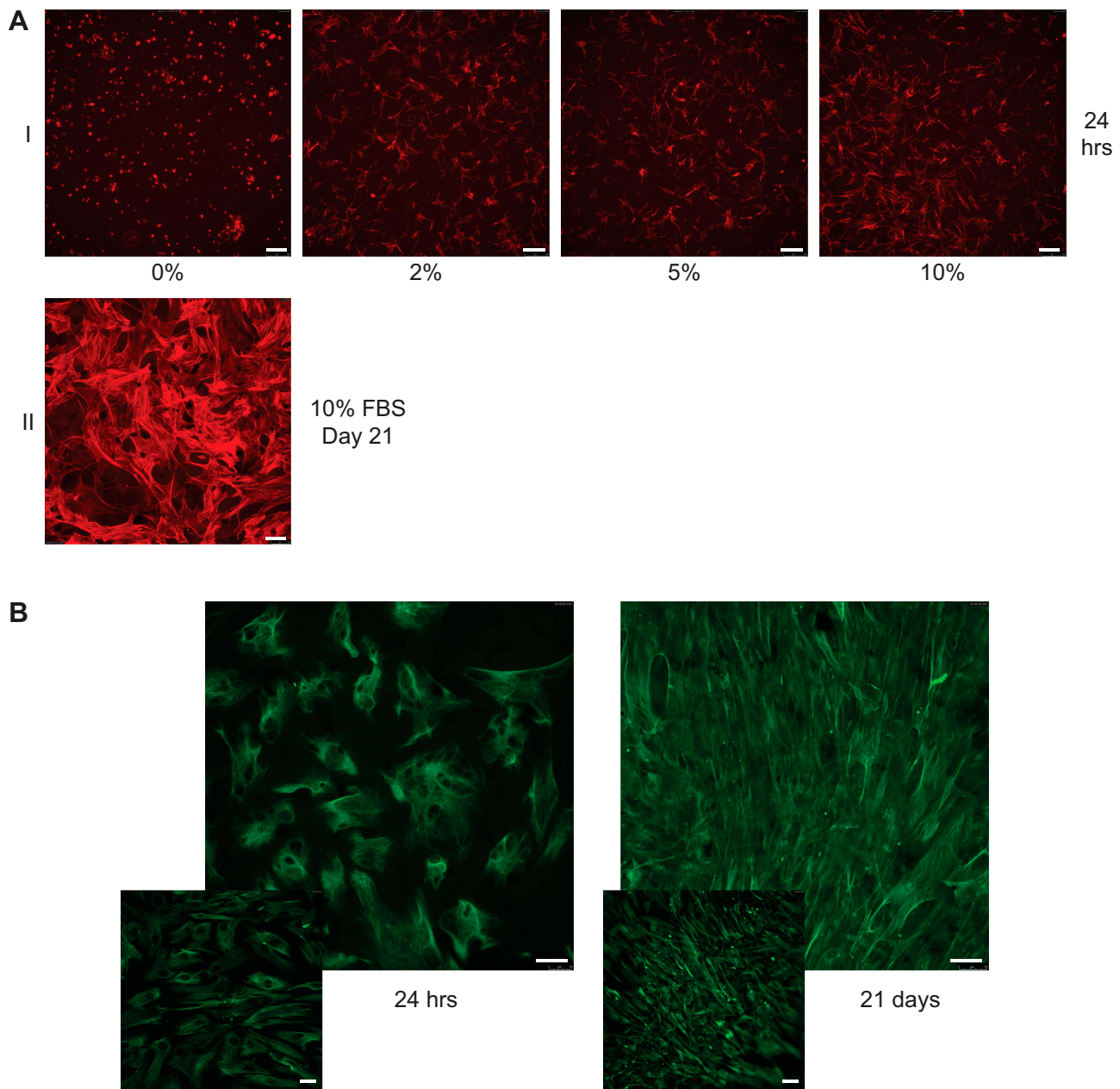


Figure 5 Cytoskeletal integrity, cell morphology, and cell identity. **(A)** Alexa fluor 594 conjugated phalloidin was used to evaluate cytoskeletal integrity and cell morphology of human mesenchymal stem cells (hMSCs) when they were seeded on low-oxygen graphene (LOG) in presence of growth media containing 0, 2, 5, 10% fetal bovine serum (FBS). Cells were fixed with 4% paraformaldehyde after 24 hrs and stained to visualize F-actin (I). Cells were incubated on LOG surface for 21 days in 10%FBS containing media to ensure that the cell integrity and morphology are maintained during the 3-week period of osteogenic differentiation (II). **(B)** Expression of vimentin in hMSCs confirmed their identity. Vimentin was used to image cells during cell adhesion ie within 24 hrs (I) and differentiation ie at day 21 (II) on low-oxygen graphene (LOG) surfaces. The insets show fluorescent staining of hMSCs on tissue culture polystyrene surface.

proteins and provide clues to the integrin-ECM protein interactions on graphene substrate.

Another important observation from our experiments is that in the presence of LOG substrates, hMSCs underwent osteogenesis spontaneously without any osteogenic inducers. These results prove our hypothesis that the surface chemistry and topography of LOG nanoparticles create an

osteogenic niche for hMSCs, at least in part by inducing integrin and specific ECM proteins' interaction, and thus, eliminating the need for osteogenic inducing agents.

Graphene nanocomposites that are being developed for bone tissue engineering are intended to serve as ECM analogs, but little is known about the mechanisms by which they regulate cell function. It is possible that similar

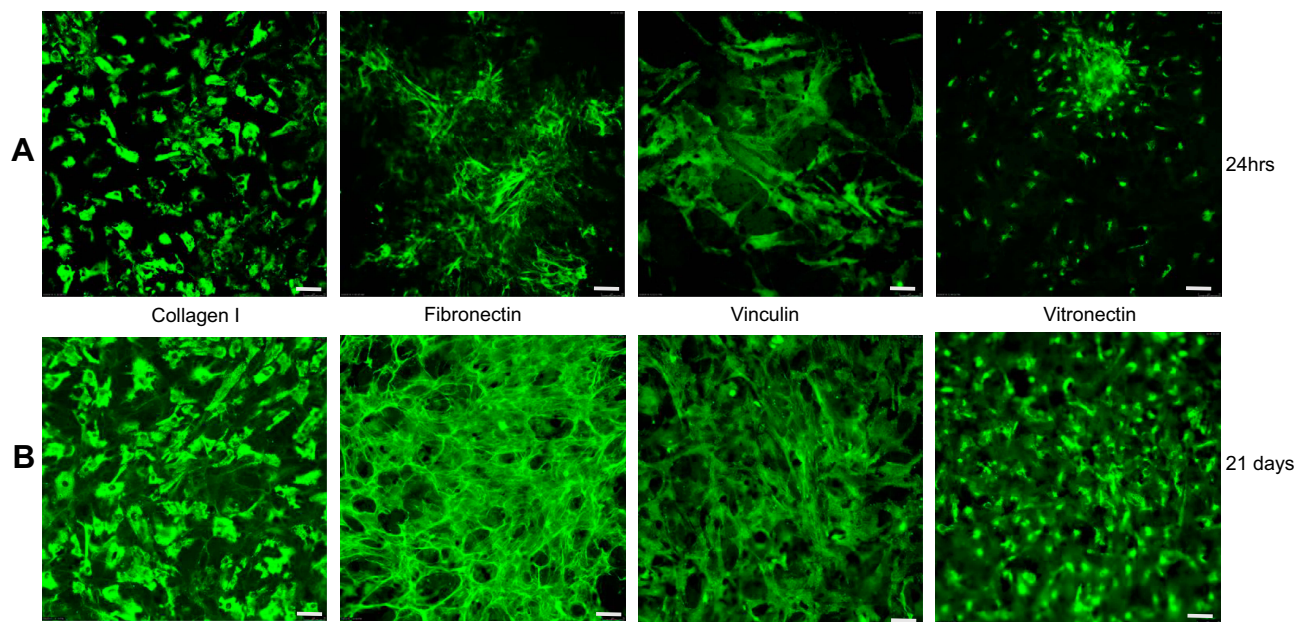


Figure 6 Expression of extracellular matrix proteins. Proteins expressed during cell adhesion ie within 24 hrs (**A**) and differentiation ie at day 21 (**B**) were assessed using immunofluorescence assays.

to gold nanoparticles, graphene nanoparticles may interact with the ECM to up-regulate β 1-integrin, generate mechanical stress on the MSCs resulting in activation of the p38 MAPK pathway, and, in turn, may induce spontaneous osteogenic differentiation.^{31,50,51} Furthermore, osteogenic inducers included in the growth media may create an osteogenic environment for MSCs to commit towards osteoblast lineage. The expression of specific ECM proteins by hMSCs on LOG surfaces potentially provides cues for cells to undergo osteogenic differentiation, the exact signaling mechanism(s) of which needs to be elucidated.

One major challenge in bone tissue engineering is to develop novel scaffolds capable of controlling cell fate. This is the essence of biomimicry. Besides biochemical stimuli, physical properties of scaffolds including, surface patterns, elasticity and nano-topography have been shown to affect osteogenic differentiation of MSCs.^{52–54} It is possible that the areas of cell clustering observed on LOG nanoparticles overlap with areas of increased surface roughness, and provide an ideal niche for anchoring, proliferation, and potentially osteogenic differentiation and mineralization. Published research supports that rough surfaces allow cells to attach more easily due to the multiple sites for cell–surface interaction and increasing cytoskeletal stresses result in the recruitment of more adhesive molecules.^{55,56} The results of the studies reported herein demonstrate that osteogenesis may be partially due to the

rough topography of LOG nanoparticles, further supported by published studies.^{57–62}

Conclusion

Our data supports our hypothesis and confirms that the LOG nanoparticles used in these studies are cytocompatible, inductive of osteogenic differentiation and that hMSCs recognize graphene nanoparticles as biomimetic in vitro substrates for the purpose of osteogenic cell culture experiments. We demonstrate the expression of specific ECM proteins by hMSCs in response to a specific form of LOG graphene nanoparticles. The graphene nanoparticles + MSC constructs provide us with a system that can be used to understand the signaling mechanisms, or cues, that are triggered when MSCs are committed towards the osteogenic lineage. Future experiments using this system will potentially aid in exploring the mechanisms underlying osteogenesis mediated by the specific ECM proteins on LOG nanoparticles, which will further improve the applicability and the use of graphene nanoparticles in bone tissue engineering.

Acknowledgments

The authors would like to acknowledge the assistance of Ms. Amanda Hand, Communications Coordinator (University of TN) and Emily Davis, Content/Grant Writer (University of Arkansas at Little Rock) for English language editing. This work was supported by grants from NIH/NIAMS

(R15AR070460) to MD, and partial support from FDA (Contract # HSF223201400079C – Arkansas Research Alliance) to SEB.

Disclosure

The authors report no conflicts of interest in this work.

References

- Sanz-Herrera JA, Reina-Romo E. Cell-biomaterial mechanical interaction in the framework of tissue engineering: insights, computational modeling and perspectives. *Int J Mol Sci.* 2011;12(11):8217–8244. doi:10.3390/ijms12118217
- Bieback K, Kern S, Kocaomer A, Ferlik K, Bugert P. Comparing mesenchymal stromal cells from different human tissues: bone marrow, adipose tissue and umbilical cord blood. *Biomed Mater Eng.* 2008;18(1 Suppl):S71–S76.
- Caplan AI. Adult mesenchymal stem cells for tissue engineering versus regenerative medicine. *J Cell Physiol.* 2007;213(2):341–347. doi:10.1002/(ISSN)1097-4652
- Dominici M, Le Blanc K, Mueller I, et al. Minimal criteria for defining multipotent mesenchymal stromal cells. The International Society for Cellular Therapy position statement. *Cytotherapy.* 2006;8(4):315–317. doi:10.1080/14653240600855905
- Pittenger MF. Mesenchymal stem cells from adult bone marrow. *Methods Mol Biol.* 2008;449:27–44. doi:10.1007/978-1-60327-169-1_2
- Assis-Ribas T, Forni MF, Winnischofer SMB, Sogayar MC, Trombetta-Lima M. Extracellular matrix dynamics during mesenchymal stem cells differentiation. *Dev Biol.* 2018;437(2):63–74. doi:10.1016/j.ydbio.2018.03.002
- Carvalho MS, Silva JC, Cabral JMS, da Silva CL, Vashishth D. Cultured cell-derived extracellular matrices to enhance the osteogenic differentiation and angiogenic properties of human mesenchymal stem/stromal cells. *J Tissue Eng Regen Med.* 2019;13(9):1544–1558. doi:10.1002/term.2907
- Daley WP, Peters SB, Larsen M. Extracellular matrix dynamics in development and regenerative medicine. *J Cell Sci.* 2008;121(Pt 3):255–264. doi:10.1242/jcs.006064
- Frantz C, Stewart KM, Weaver VM. The extracellular matrix at a glance. *J Cell Sci.* 2010;123(Pt 24):4195–4200. doi:10.1242/jcs.023820
- Gattazzo F, Urciuolo A, Bonaldo P. Extracellular matrix: a dynamic microenvironment for stem cell niche. *Biochim Biophys Acta.* 2014;1840(8):2506–2519. doi:10.1016/j.bbagen.2014.01.010
- Felgueiras HP, Evans MDM, Migonney V. Contribution of fibronectin and vitronectin to the adhesion and morphology of MC3T3-E1 osteoblastic cells to poly(NaSS) grafted Ti6Al4V. *Acta Biomater.* 2015;28:225–233.
- Bays JL, DeMali KA. Vinculin in cell-cell and cell-matrix adhesions. *Cell Mol Life Sci.* 2017;74(16):2999–3009. doi:10.1007/s00018-017-2511-3
- Alford AI, Kozloff KM, Hankenson KD. Extracellular matrix networks in bone remodeling. *Int J Biochem Cell Biol.* 2015;65:20–31. doi:10.1016/j.biocel.2015.05.008
- He J, Jiang B, Dai Y, et al. Regulation of the osteoblastic and chondrocytic differentiation of stem cells by the extracellular matrix and subsequent bone formation modes. *Biomaterials.* 2013;34(28):6580–6588. doi:10.1016/j.biomaterials.2013.05.056
- Wan Y, Lu C, Cao J, et al. Osteoblastic Wnts differentially regulate bone remodeling and the maintenance of bone marrow mesenchymal stem cells. *Bone.* 2013;55(1):258–267. doi:10.1016/j.bone.2012.12.052
- Curry AS, Pensa NW, Barlow AM, Bellis SL. Taking cues from the extracellular matrix to design bone-mimetic regenerative scaffolds. *Matrix Biol.* 2016;52–54:397–412. doi:10.1016/j.matbio.2016.02.011
- Khademhosseini A, Vacanti JP, Langer R. Progress in tissue engineering. *Sci Am.* 2009;300(5):64–71. doi:10.1038/scientificamerican0509-64
- Kundu AK, Khatiwala CB, Putnam AJ. Extracellular matrix remodeling, integrin expression, and downstream signaling pathways influence the osteogenic differentiation of mesenchymal stem cells on poly(lactide-co-glycolide) substrates. *Tissue Eng Part A.* 2009;15(2):273–283. doi:10.1089/ten.tea.2008.0055
- Mistry AS, Mikos AG. Tissue engineering strategies for bone regeneration. *Adv Biochem Eng Biotechnol.* 2005;94:1–22.
- Grattoni A, Tasciotti E, Fine D, et al. Nanotechnologies and regenerative medical approaches for space and terrestrial medicine. *Aviat Space Environ Med.* 2012;83(11):1025–1036. doi:10.3357/ASEM.3307.2012
- Nosouhian S, Razavi M, Jafari-Pozve N, Rismanchian M. Comparative evaluation of hydroxyapatite and nano-bioglass in two forms of conventional micro- and nano-particles in repairing bone defects (an animal study). *Indian J Dent Res.* 2015;26(4):366–371. doi:10.4103/0970-9290.167645
- Zhang ZG, Li ZH, Mao XZ, Wang WC. Advances in bone repair with nanobiomaterials: mini-review. *Cytotechnology.* 2011;63(5):437–443. doi:10.1007/s10616-011-9367-4
- Dubey N, Bentini R, Islam I, Cao T, Castro Neto AH, Rosa V. Graphene: a versatile carbon-based material for bone tissue engineering. *Stem Cells Int.* 2015;2015:804213. doi:10.1155/2015/804213
- Majeed W, Bourdo S, Petibone DM, et al. The role of surface chemistry in the cytotoxicity profile of graphene. *J Appl Toxicol.* 2017;37(4):462–470. doi:10.1002/jat.v37.4
- Mao HY, Laurent S, Chen W, et al. Graphene: promises, facts, opportunities, and challenges in nanomedicine. *Chem Rev.* 2013;113(5):3407–3424. doi:10.1021/cr300335p
- Zhang B, Wang Y, Zhai G. Biomedical applications of the graphene-based materials. *Mat Sci Eng C.* 2016;61:953–964. doi:10.1016/j.msec.2015.12.073
- Zhang B, Wei P, Zhou Z, Wei T. Interactions of graphene with mammalian cells: molecular mechanisms and biomedical insights. *Adv Drug Deliv Rev.* 2016;105(Pt B):145–162. doi:10.1016/j.addr.2016.08.009
- Dervishi E, Li ZR, Watanabe F, et al. Large-scale graphene production by RF-cVD method. *Chem Commun.* 2009;(27):4061–4063. doi:10.1039/b906323d
- Elkhenany H, Amelse L, Lafont A, et al. Graphene supports in vitro proliferation and osteogenic differentiation of goat adult mesenchymal stem cells: potential for bone tissue engineering. *J Appl Toxicol.* 2015;35(4):367–374. doi:10.1002/jat.v35.4
- Mahmood M, Casciano DA, Mocan T, et al. Cytotoxicity and biological effects of functional nanomaterials delivered to various cell lines. *J Appl Toxicol.* 2010;30(1):74–83. doi:10.1002/(ISSN)1099-1263
- Nayak TR, Andersen H, Makam VS, et al. Graphene for controlled and accelerated osteogenic differentiation of human mesenchymal stem cells. *ACS Nano.* 2011;5(6):4670–4678. doi:10.1021/nn200500h
- Nayak TR, Jian L, Phua LC, Ho HK, Ren YP, Pastorin G. Thin films of functionalized multiwalled carbon nanotubes as suitable scaffold materials for stem cells proliferation and bone formation. *ACS Nano.* 2010;4(12):7717–7725. doi:10.1021/nn102738c
- Wang K, Ruan J, Song H, et al. Biocompatibility of graphene oxide. *Nanoscale Res Lett.* 2011;6.
- Mahmood MV, Dervishi HE, et al. Role of the carbonaceous nanomaterials in stimulation of osteogenesis in mammalian bone cells. *J Mat Chem B.* 2013;25:3220–3230.
- Majeed W, Bourdo S, Petibone DM, et al. The role of surface chemistry in the cytotoxicity profile of graphene. *J Appl Toxicol.* 2016;37(4).
- Jeong JT, Choi MK, Sim Y, et al. Effect of graphene oxide ratio on the cell adhesion and growth behavior on a graphene oxide-coated silicon substrate. *Sci Rep.* 2016;6:33835. doi:10.1038/srep33835

37. Elkhenany H, Bourdo S, Hecht S, et al. Graphene nanoparticles as osteoinductive and osteoconductive platform for stem cell and bone regeneration. *Nanomedicine*. 2017;13(7):2117–2126. doi:10.1016/j.nano.2017.05.009
38. Bourdo SE, Al Faouri R, Sleezer R, et al. Physicochemical characteristics of pristine and functionalized graphene. *J Appl Toxicol*. 2017;37(11):1288–1296. doi:10.1002/jat.v37.11
39. Alghazali KM, Newby SD, Nima ZA, et al. Functionalized gold nanorod nanocomposite system to modulate differentiation of human mesenchymal stem cells into neural-like progenitors. *Sci Rep*. 2017;7(1):16654. doi:10.1038/s41598-017-16800-9
40. Feoktistova M, Geserick P, Leverkus M. Crystal violet assay for determining viability of cultured cells. *Cold Spring Harb Protoc*. 2016;2016(4):pdb prot087379. doi:10.1101/pdb.prot087379
41. Bow A, Newby S, Rifkin R, et al. Evaluation of a polyurethane platform for delivery of nanohydroxyapatite and decellularized bone particles in a porous three-dimensional scaffold. *ACS Appl Bio Mater*. 2019;2(5):1815–1829. doi:10.1021/acsabm.8b00670
42. Elkhenany H, Amelse L, Caldwell M, Abdelwahed R, Dhar M. Impact of the source and serial passaging of goat mesenchymal stem cells on osteogenic differentiation potential: implications for bone tissue engineering. *J Anim Sci Biotechnol*. 2016;7:16. doi:10.1186/s40104-016-0074-z
43. Datsyuk V, Kalyva M, Papagelis K, et al. Chemical oxidation of multiwalled carbon nanotubes. *Carbon*. 2008;46:833–840. doi:10.1016/j.carbon.2008.02.012
44. Yang D, Velamakanni A, Bozoklu G, et al. Chemical analysis of graphene oxide films after heat and chemical treatments by X-ray photoelectron and Micro-Raman spectroscopy. *Carbon*. 2009;47:145–152. doi:10.1016/j.carbon.2008.09.045
45. Malarid LM, Pimenta MA, Dresselhaus G, Dresselhaus MS. Raman spectroscopy in graphene. *Phys Rep*. 2009;473(5–6):51–87. doi:10.1016/j.physrep.2009.02.003
46. Wojtoniszak M, Chen XC, Kalenczuk RJ, et al. Synthesis, dispersion, and cytocompatibility of graphene oxide and reduced graphene oxide. *Colloid Surf B*. 2012;89:79–85. doi:10.1016/j.colsurfb.2011.08.026
47. Nima ZA, Vang KB, Nedosekin D, et al. Quantification of cellular associated graphene and induced surface receptor responses. *Nanoscale*. 2019;11(3):932–944. doi:10.1039/C8NR06847J
48. Secunda R, Vennila R, Mohanashankar AM, Rajasundari M, Jeswanth S, Surendran R. Isolation, expansion and characterisation of mesenchymal stem cells from human bone marrow, adipose tissue, umbilical cord blood and matrix: a comparative study. *Cytotechnology*. 2015;67(5):793–807. doi:10.1007/s10616-014-9718-z
49. Jackson BK, Bow AJ, Kannarpady G, et al. Polyurethane/nanohydroxyapatite composite films as osteogenic platforms. *J Biomater Sci Polym Ed*. 2018;29(12):1426–1443. doi:10.1080/09205063.2018.1464264
50. Yi C, Liu D, Fong CC, Zhang J, Yang M. Gold nanoparticles promote osteogenic differentiation of mesenchymal stem cells through p38 MAPK pathway. *ACS Nano*. 2010;4(11):6439–6448. doi:10.1021/nn101373r
51. Zhang R, Lee P, Lui VC, et al. Silver nanoparticles promote osteogenesis of mesenchymal stem cells and improve bone fracture healing in osteogenesis mechanism mouse model. *Nanomedicine*. 2015;11(8):1949–1959. doi:10.1016/j.nano.2015.07.016
52. Qian W, Gong L, Cui X, et al. Nanotopographic regulation of human mesenchymal stem cell osteogenesis. *ACS Appl Mater Interfaces*. 2017;9(48):41794–41806. doi:10.1021/acsami.7b16314
53. Goriainov V, Hulsart-Billstrom G, Sjoström T, Dunlop DG, Su B, Oreffo ROC. Harnessing nanotopography to enhance osseointegration of clinical orthopedic titanium implants—an in vitro and in vivo analysis. *Front Bioeng Biotechnol*. 2018;6:44. doi:10.3389/fbioe.2018.00044
54. Metavarayuth K, Maturavongsadit P, Chen X, et al. Nanotopographical cues mediate osteogenesis of stem cells on virus substrates through BMP-2 intermediate. *Nano Lett*. 2019;19(12):8372–8380. doi:10.1021/acs.nanolett.9b02001
55. Gentile F, Tirinato L, Battista E, et al. Cells preferentially grow on rough substrates. *Biomaterials*. 2010;31(28):7205–7212. doi:10.1016/j.biomaterials.2010.06.016
56. Tang LA, Lee WC, Shi H, et al. Highly wrinkled cross-linked graphene oxide membranes for biological and charge-storage applications. *Small*. 2012;8(3):423–431. doi:10.1002/sml.201101690
57. Deng Y, Liu X, Xu A, et al. Effect of surface roughness on osteogenesis in vitro and osseointegration in vivo of carbon fiber-reinforced polyetheretherketone-nanohydroxyapatite composite. *Int J Nanomedicine*. 2015;10:1425–1447. doi:10.2147/IJN.S75557
58. Wang S, Deng Z, Ye X, Geng X, Zhang C. Enterococcus faecalis attenuates osteogenesis through activation of p38 and ERK1/2 pathways in MC3T3-E1 cells. *Int Endod J*. 2016;49(12):1152–1164. doi:10.1111/iej.2016.49.issue-12
59. Xu A, Liu X, Gao X, Deng F, Deng Y, Wei S. Enhancement of osteogenesis on micro/nano-topographical carbon fiber-reinforced polyetheretherketone-nanohydroxyapatite biocomposite. *Mater Sci Eng C Mater Biol Appl*. 2015;48:592–598. doi:10.1016/j.msec.2014.12.061
60. Damiani L, Eales MG, Nobbs AH, et al. Impact of surface topography and coating on osteogenesis and bacterial attachment on titanium implants. *J Tissue Eng*. 2018;9:2041731418790694. doi:10.1177/2041731418790694
61. Zhang Y, Chen SE, Shao J, van den Beucken J. Combinatorial surface roughness effects on osteoclastogenesis and osteogenesis. *ACS Appl Mater Interfaces*. 2018;10(43):36652–36663. doi:10.1021/acsami.8b10992
62. Zhang T, Lin S, Shao X, et al. Regulating osteogenesis and adipogenesis in adipose-derived stem cells by controlling underlying substrate stiffness. *J Cell Physiol*. 2018;233(4):3418–3428. doi:10.1002/jcp.26193

International Journal of Nanomedicine

Publish your work in this journal

The International Journal of Nanomedicine is an international, peer-reviewed journal focusing on the application of nanotechnology in diagnostics, therapeutics, and drug delivery systems throughout the biomedical field. This journal is indexed on PubMed Central, MedLine, CAS, SciSearch®, Current Contents®/Clinical Medicine,

Submit your manuscript here: <https://www.dovepress.com/international-journal-of-nanomedicine-journal>

Dovepress

Journal Citation Reports/Science Edition, EMBASE, Scopus and the Elsevier Bibliographic databases. The manuscript management system is completely online and includes a very quick and fair peer-review system, which is all easy to use. Visit <http://www.dovepress.com/testimonials.php> to read real quotes from published authors.